Journal of the Korean Ceramic Society (2021) 58:116–122
https://doi.org/10.1007/s43207-020-00087-0

ORIGINAL ARTICLE

Characterization of nanosized hydroxyapatite prepared by an aqueous precipitation method using eggshells and mulberry leaf extract

Shih-Ching Wu[1] · Hsueh-Chuan Hsu[1] · Mei-Yi Liu[2] · Wen-Fu Ho[2]

Received: 15 August 2020 / Revised: 24 September 2020 / Accepted: 29 September 2020 / Published online: 14 October 2020

Abstract

Hydroxyapatite (HA) has been vigorously studied for orthopedic and dental applications due to its excellent bioactivity, osteoconductivity, and osteoinductivity. This study aims to present a simple room-temperature aqueous precipitation method for obtaining carbonated HA nanoparticles of high purity from biowaste chicken eggshells. Biowaste chicken eggshells were used for preparing HA through aqueous precipitation method. Moreover, mulberry leaf extract was used as a template to regulate the morphology, size, and crystallinity of HA. All produced nanocrystalline HA powders exhibited rod-like particle agglomerates of a size below 100 nm. The HA particles synthesized with the mulberry leaf extract showed higher crystallinity and slightly decreased crystallite sizes compared to the samples prepared without adding the extract. Carbonate peaks observed for the specimens closely matched those of A- and B-type carbonates, which can contribute to the low crystallinity. Notably, the HA synthesized from the eggshell powders contains several important trace elements such as Mg and Sr, which are beneficial to the overall biological performance as biomaterials. The morphology, size, structure, and composition of the obtained HA products are similar to those of natural bones, and consequently, the products show potential as a material for biomedical applications.

Keywords Eggshell · Hydroxyapatite · Nanoparticles · Aqueous precipitation method

1 Introduction

Hydroxyapatite [HA, $Ca_{10}(PO_4)_6(OH)_2$], the major component of human bones, has been widely used in medical and dental applications because of its superior biocompatibility, osteoconductivity, and bioactivity [1]. Generally, HA is used in the coating of metallic implants, alveolar bridge augmentation, orthopedics, maxillofacial surgery, and drug delivery systems [2]. In addition, it has been applied as a host material for lasers, gas sensors, and catalysts [3]. The biological and mechanical properties of synthetic HA are strongly influenced by its particle size, morphology, chemical composition, and crystalline structure, which depend on synthesis parameters [4].

Mineral crystals in human bones are nanosized with a very large surface area. Their compositions differ slightly from stoichiometric HA because of the presence of impurities such as carbonate, chloride, magnesium, and strontium in human bones. In particular, natural bones contain carbonated HA with 2–8% carbonate by weight [5–7]. Recently, nanocrystalline HA (nano-HA) has attracted attention because of its excellent biocompatibility, affinity for biopolymers, and high levels of osteoconduction and osteointegration [8, 9]. A recent study also showed retardant effects of nano-HA particles on cancer cells [10]. Therefore, the development of nano-HA powders with a precise control over particle size, morphology, crystallinity, and chemical composition is becoming increasingly important. In the past decade, nano-HA powders have been synthesized using various methods such as solid-state reactions, aqueous precipitation, sol–gel, and hydrothermal reactions [11–15].

Recently, considerable interest has arisen in a natural-resource-based approach to the design and manufacture of nanobiomaterials because of their availability, low cost, and

✉ Wen-Fu Ho
fujii@nuk.edu.tw

[1] Department of Dental Technology and Materials Science, Central Taiwan University of Science and Technology, Taichung 40601, Taiwan

[2] Department of Chemical and Materials Engineering, National University of Kaohsiung, 700 Kaohsiung University Rd., Nanzih District, Kaohsiung 81148, Taiwan

eco-friendliness. In this study, eggshell biowaste was used as the Ca source for preparing nano-HA powders using the aqueous precipitation method. The eggshell contains several trace elements, which remain in the synthesized HA powder, making it akin to human bones. In addition, the mulberry leaf extract was added as a template. In the past decade, biopolymers such as collagens, gelatin, and peptides have attracted extensive interest regarding the regulation of the morphology, size, and crystallinity of HA [16–18]. In the present study, the natural mulberry leaf extract used is biodegradable, biocompatible, water soluble, and inexpensive in comparison to other biodegradable polymers. Moreover, it has been shown to inhibit oxidative modification of low-density lipoproteins [19] and displays anti-inflammatory effects, suppressing the proinflammatory gene expression [20]. The prepared HA powders were characterized by X-ray diffraction, scanning electron microscopy, and Fourier transform infrared spectroscopy to explore their structural properties.

2 Materials and methods

Eggshells were collected, cleaned thoroughly with water, dried overnight at 45 °C in an oven, and then crushed and powdered using an agate mortar. Thereafter, 2 g of the resulting powder was dissolved in 20 ml of a 1:3 hydrochloric acid/water solution. Then, 0.1 g of the mulberry leaf extract was added to 20 ml of the above eggshell solution and stirred gently but thoroughly. Subsequently, 0.8 ml (i.e., Ca/P molar ratio = 1.67) of 85% phosphoric acid was added gradually to the stirred mixture. Ammonium hydroxide was used to adjust the pH to 10. To study the effect of the mulberry leaf extract on the characteristics of synthesized HA, a solution without the extract was used as a control. All reactions were aged independently at room temperature over different reaction times (10 min, 1 h, and 24 h). Thereafter, the obtained powder was separated from the liquid phase by filtration, rinsed with deionized water, and dried at 45 °C for 24 h prior to examination.

Sample phases were identified by X-ray diffraction (XRD) with Cu Kα radiation (XRD-6000, Shimadzu, Japan). The phases were identified by comparing experimental X-ray diffractograms to standards compiled by the Joint Committee on Powder Diffraction Standards. The morphology of the microstructure was studied by field emission scanning electron microscopy (FE-SEM; JSM-7401F, JEOL, Japan). Mean particle dimensions were estimated by an image analysis of SEM micrographs. For this purpose, the dimensions of all samples were calculated from the measurements of 30 randomly selected individual particles. The elemental compositions of the products were qualitatively identified by energy-dispersive X-ray spectroscopy (EDS) in the SEM. FTIR (FTS-40, Bio-Rad, USA) was performed in the region of 600–4000 cm^{-1} on the powdered samples. To gain information on the phase transformation of the obtained HA, thermal analysis (TG–DTA; SDT-Q600, TA Inc., USA) was performed in a nitrogen atmosphere from room temperature to 1400 °C at a heating rate of 10 °C/min. To evaluate the composition of the synthesized powders and the presence of heavy metals, inductively coupled plasma atomic emission spectrometry (ICP-AES; 725, Agilent Co., USA) analysis was performed.

From the XRD data, the crystallinity (X_c) of the HA particles was calculated according to the equation as follows [21]:

$$X_c = 1 - \frac{V_{112/300}}{I_{300}},$$

where I_{300} is the intensity of (300) diffraction peak and $V_{112/300}$ is the intensity of the hollow between (112) and (300) diffraction peaks of HA.

The crystallite sizes of the synthesized HA particles can be evaluated by measuring the full width at half maximum (FWHM) according to the Scherrer formula [22]:

$$X_s = \frac{0.9\lambda}{\mathrm{FWHM}\ \cos\theta},$$

where X_s is the average crystallite size (nm), λ is the wavelength of X-ray radiation (1.5406 Å), FWHM is for the diffraction peak under consideration (rad), and θ (degree) is the Bragg angle. The (002) diffraction peak was selected for the calculation of the crystal size because it was isolated and sharper than others and showed the crystal growth along the c axis of the HA crystalline structure.

3 Results and discussion

3.1 X-ray diffraction analysis

XRD patterns of the HA powders synthesized with and without the mulberry leaf extract by aqueous precipitation at room temperature for different reaction times (10 min, 1 h, and 24 h) are shown in Fig. 1. As can be observed, the HA powders synthesized with and without the mulberry leaf extract have similar XRD patterns. All major peaks of HA are evident in the XRD patterns without any unknown peaks, indicating that all samples were predominantly HA and the use of the mulberry leaf extract did not hinder the formation of HA phases. These six XRD patterns showed broad diffraction peaks, suggesting a poorly crystallized HA phase. The presence of these broad peaks may show that tiny crystallites of HA were formed. Accordingly, the crystallographic structure of the synthesized HA is similar to that of natural bones.

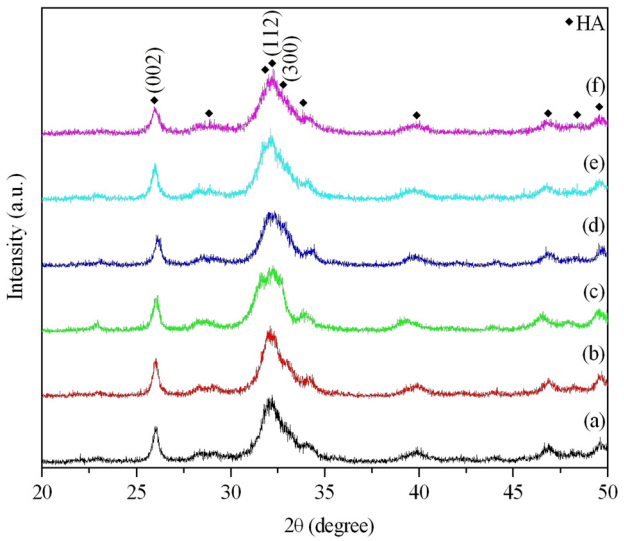

Fig. 1 XRD patterns of the HA powders synthesized with and without the mulberry leaf extract by aqueous precipitation at room temperature for different reaction times. **a** Without mulberry leaf, 10 min, **b** without mulberry leaf, 1 h, **c** without mulberry leaf, 24 h, **d** with mulberry leaf, 10 min, **e** with mulberry leaf, 1 h, **f** with mulberry leaf, 24 h

The crystallinity of the synthesized HA particles was calculated from the XRD data, as shown in Table 1. For each type of the HA powder with and without the mulberry leaf extract, the crystallinity of the synthesized particles slightly increased with the increasing aging time. The samples prepared using the mulberry leaf extract showed higher crystallinity. The poorly crystalline nature of the prepared HA may be due to the low-temperature process used in this study. This structure is expected to be more active under a metabolic activity than the fully developed crystalline HA structure, which is considered to be nonsoluble in the physiological environment [23]. In addition, the crystallite sizes of the synthesized HA powders were calculated using the characteristic peak (002) by the Scherrer formula, as shown in Table 1. These results indicate that average crystallite sizes slightly increased with longer aging times and slightly decreased with the addition of the mulberry leaf extract. This is consistent with the observation of Sadjadi et al. [24], who found that nano-HA composite synthesis can be performed at room temperature by a mimetic method using wheat starch as a templating agent and the crystallite size increases as the immersion time increases. In the present study, the crystallite sizes in the obtained HA powders are 19.0–21.5 nm for the control sample and 12.6–14.3 nm for the sample prepared using the mulberry leaf extract.

3.2 Morphology and characterization

Figure 2 represents the SEM micrographs of HA prepared for different aging times in the presence and absence of the mulberry leaf extract. SEM analysis of samples revealed that the synthesized nano-HA powder exists as rod-like particle agglomerates with a size below 100 nm. The importance of nanoparticles lies in their inherently large surface-to-volume ratio relative to that of larger particles [25]. These high surface areas are accompanied by van der Waals interactions, which result in a strong tendency to agglomerate. In the control group, there was a slight increase in the size of these rod-like particles from 58.3 nm in length and 24.8 nm in diameter to 67.8 nm in length and 26.7 nm in diameter (Fig. 2a–c) when aging for 10 min to 24 h. For the synthetic HA crystals developed by adding the mulberry leaf extract (Fig. 2d–f), the particle size increased from 45.5 nm in length and 14.1 nm in diameter to 52.2 nm in length and 18.0 nm in diameter with increasing aging time from 10 min to 24 h. The sample prepared using the mulberry leaf extract showed a relatively smaller particle size in the present study.

Crystallization is a process considered in terms of nucleation and crystal growth. According to classical nucleation theory, heterogeneous nucleation always occurs earlier than homogeneous nucleation in a supersaturated solution because of the lower free energies of nuclei on the surface of foreign bodies [26]. In the present study, the mulberry leaf extract in the solution provided nucleation sites for the HA nuclei. Mineral nuclei gradually grew on the surface of the mulberry leaf extract, leading to the formation of HA crystals. The addition of the mulberry leaf extract to the Ca/P reaction solution leads to the formation of a larger number of nuclei and, therefore, smaller HA crystallite and particle sizes. Son et al. [27] obtained similar results and indicated that the size of HA nanoparticles slightly decreased when increasing the content of the β-cyclodextrin template. Moreover, the same behavior was observed in another study [28], which investigated the

Table 1 The crystallinity, crystallite size and Ca/P ratio of HA synthesized using mulberry leaf extract by aqueous precipitation at room temperature for different reaction times

Aging time	Crystallinity, X_c (%)		Crystallite size, X_s (nm)		Ca/P ratio	
	Control	Mulberry leaf	Control	Mulberry leaf	Control	Mulberry leaf
10 min	14.0	17.6	19.0	12.6	–	–
1 h	16.5	20.8	19.4	13.6	–	–
24 h	17.0	22.3	21.5	14.3	1.41	1.50

The HA prepared without using mulberry leaf extract was used as a control

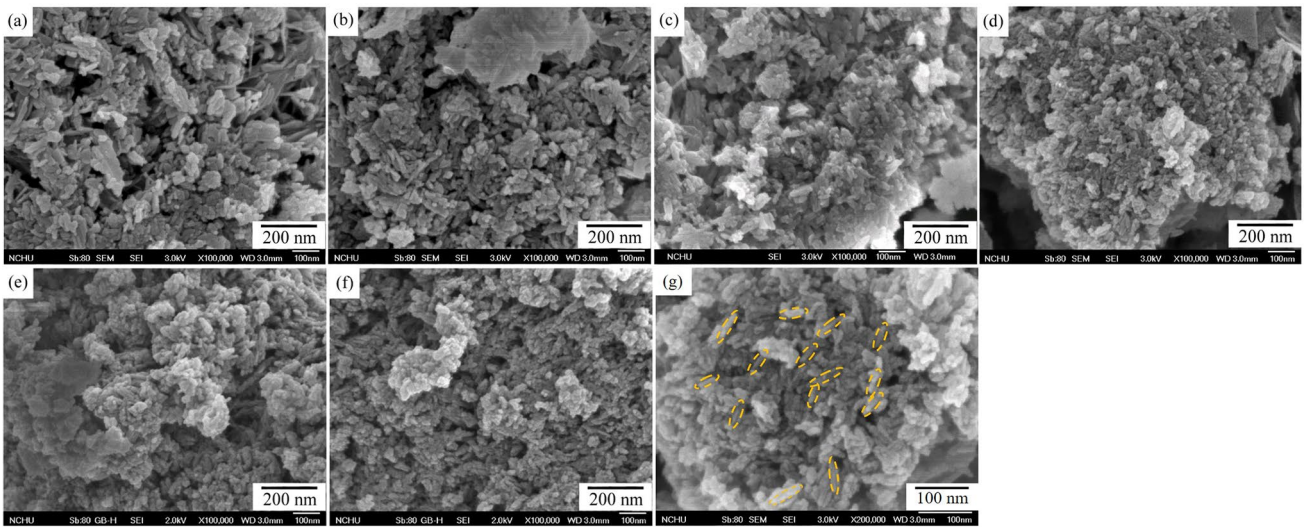

Fig. 2 SEM images of the HA powders synthesized with and without the mulberry leaf extract by aqueous precipitation at room temperature for different reaction times. **a** Without mulberry leaf, 10 min, **b** without mulberry leaf, 1 h, **c** without mulberry leaf, 24 h, **d** with mulberry leaf, 10 min, **e** with mulberry leaf, 1 h, **f** with mulberry leaf, 24 h, and **g** higher magnification with mulberry leaf, 10 min, the representative rod-shaped particles of individual HA are marked with a dashed line

morphologies of as-prepared apatite nanocrystals using heparin as a template; the results illustrated that more heparin molecules led to a bigger steric hindrance, which seriously disturbed the growth of apatite crystals. In this study, since calcium ions are easily dispersed in the solution at the molecular level, HA nanoparticles are formed through interaction with the template [27]. Therefore, the HA synthesized by adding mulberry leaf extract in this experiment has greater crystallinity and smaller grain size.

The literature reports that HA crystals in natural bones have a needle- or rod-like shape, 40–60 nm in length and 10–20 nm in width [29]. In the present study, the size of rod-like HA prepared in the presence of the mulberry leaf extract falls above the range of natural bones. The nanostructure of bone-substituting material is closely related to good bioactivity and osteoconductivity. Synthetic HA composed of nanosized crystals can lead to an increase in osteoblast functions [30].

EDS from SEM (Fig. 3 and Table 2) revealed the presence of Ca, P, O, and a small amount C in 24-h aged samples, including HA prepared in the presence and absence of the mulberry leaf extract. The Ca/P molar ratios (Table 1) calculated from the integrated intensities of Ca and P spectral lines were found to be 1.41 for the control group and 1.50 for its mulberry leaf extract counterpart, lower than the ideal ratio of 1.67. The calculated Ca/P ratio is significant and fits quite well with that of biological apatite, which ranges from 1.50 to 1.85 [31]. A small amount of C in the EDS spectrum confirms the presence of a carbonate group in the sintered sample, as shown in the FT-IR spectra.

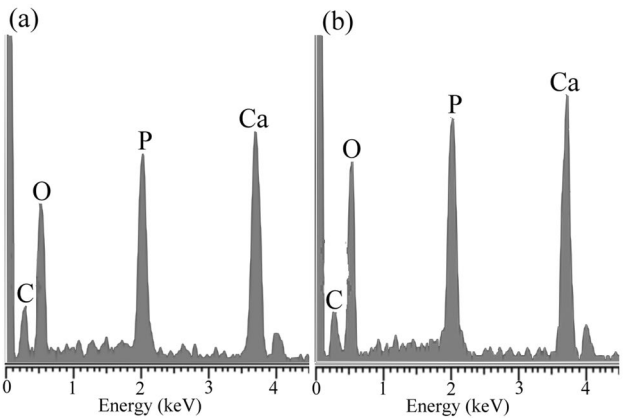

Fig. 3 EDS analyses for the HA powders synthesized with and without the mulberry leaf extract by aqueous precipitation at room temperature for 24 h. **a** Without mulberry leaf and **b** with mulberry leaf

Table 2 The chemical composition (at%) for the HA powders synthesized with and without the mulberry leaf extract by aqueous precipitation at room temperature for 24 h

Element	Control	Mulberry leaf
Ca	10.00	15.85
P	7.07	10.60
O	60.06	51.76
C	22.87	21.79

Measurements of elemental composition by the ICP-AES method showed the presence of Ca (31.2 wt%), P (14.7 wt%), Mg (0.329 wt%), and Sr (0.038 wt%) in the synthesized HA using mulberry leaf extract after 24 h. Biological HA obtained from biowaste eggshells has the advantage of preserving the chemical elements of the precursor material. The presence of several trace elements does not alter the basic crystallographic characteristics of HA but can improve the overall biological performance of the implant material [32, 33]. The presence of these ions is usual in biological apatites (Table 2). These elements play an essential role in the behavior of biological apatites since they contribute to metabolism in the human body and cell adhesion. For example, Mg plays an important role in bone metabolism, and its depletion causes bone fragility and bone loss [34]. Sr increases osteoblast replication, differentiation, and bone matrix mineralization [35, 36]. Sr has also been experimentally incorporated into calcium phosphates and bioactive glasses to enhance bone formation [36, 37]. Consequently, Mg and Sr present in the HA structure are of great interest for the development of artificial bones.

In the process of HA synthesis, the mulberry leaf extract plays a role as a template. However, it is not necessary to remove it in the final product. The HA product with mulberry leaf extract can exert its anti-inflammatory effect, which can contribute to its clinical performance when used as a bone filling material.

3.3 Fourier transform infrared analysis

Figure 4 shows FT-IR spectra of HA synthesized for 24 h in the presence and absence of the mulberry leaf extract. Both HA powders have similar FT-IR spectra, indicating that they have the same functional groups present in the HA nanoparticles. The bands assigned to OH^-, PO_4^{3-}, CO_3^{2-}, and H_2O are present. FT-IR peaks at 1059 cm^{-1} are due to PO_4^{3-}. The peak positions for the OH^- group are at 704, 3742, and 3854 cm^{-1}. The bands at 2851 and 2920 cm^{-1} are attributed to the asymmetric stretching of CH_2 and CH_3 [38]. Also, bands corresponding to CO_3^{2-} can be seen at 880, 1406, and 1527 cm^{-1}, suggesting that the powder may have a carbonate-substituted HA structure. Carbonate groups can partially substitute for OH^- (A-type) and/or PO_4^{3-} (B-type) in the lattice of synthetic HA [39]. In the present study, the peak at 1406 cm^{-1} was characteristic for B-type carbonate-containing HA, while A-type carbonates were characterized by peaks at 880 and 1527 cm^{-1}. Bony natural apatites contain carbonate ions in significant amounts, from about 2–8 wt% [40]. In general, carbonated HA shows favorable biological properties and is reported to have an appropriate absorbance time period and good bone formation ability [41].

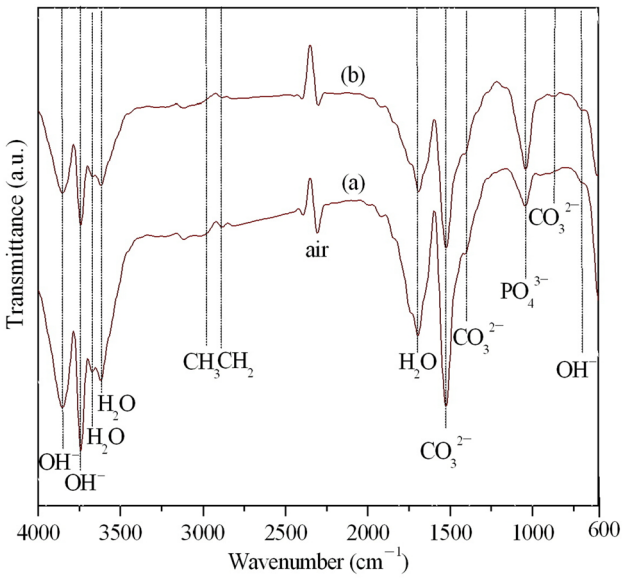

Fig. 4 FT-IR spectra of the HA powders synthesized with and without the mulberry leaf extract by aqueous precipitation at room temperature for 24 h. **a** Without mulberry leaf and **b** with mulberry leaf

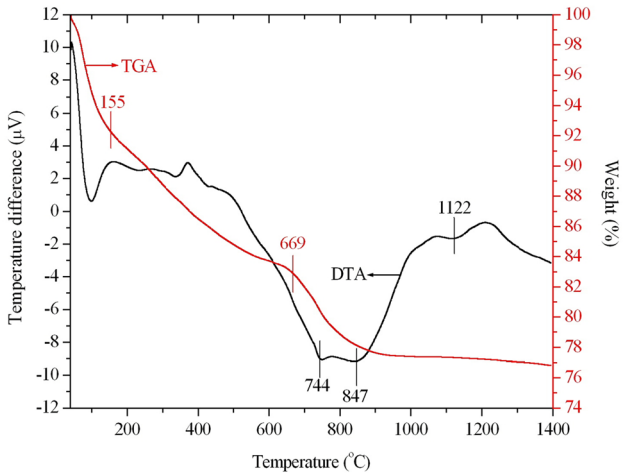

Fig. 5 TGA and DTA curves of the HA powders synthesized with the mulberry leaf extract by aqueous precipitation at room temperature for 24 h

3.4 Thermal behavior

It is necessary to study the thermal behavior of the synthesized nano-HA powder because nano-HA can be used in various forms such as powder/particulate for drug delivery, filling bone voids, or coating metallic prostheses, especially in the temperature range 400–1200 °C [42]. Figure 5 shows the TGA/DTA thermogram of the as-prepared HA powder with the added mulberry leaf extract synthesized by aqueous precipitation at room temperature for 24 h. The TGA curve

of the as-prepared HA showed that the weight loss occurring up to around 155 °C was caused by the release of physically adsorbed and interstitial H_2O molecules, while the weight loss in the range of 155–669 °C was due to the removal of crystallized water. In the DTA curve, an endothermic peak at 744 °C could be explained as a result of gradual dehydroxylation and/or decarboxylation of the HA phase, which was also observed by Zhang et al. [43]. An endothermic peak was detected at around 847 °C, which was estimated to be the phase transformation of HA into the β-TCP phase, whereas the last peak involves the decomposition of HA/β-TCP to the α-TCP phase [44, 45].

4 Conclusions

This is the first report on the production of nanosized carbonated HA powders by the aqueous precipitation method at room temperature using eggshell waste as the Ca source and adding mulberry leaf extract as a template. Our results indicate the following important points:

1. The HA powders that were synthesized with and without the mulberry leaf extract show similar XRD patterns and no other crystalline phase is observed besides HA. The broad peaks in the XRD patterns point out the tiny size and poor crystallinity of the HA, which is similar to a natural bone mineral.
2. The crystallinity of the synthesized HA particles increased slightly with an increase in aging time from 10 min to 24 h, and the samples prepared using the mulberry leaf extract displayed higher crystallinity. In addition, average crystallite sizes were slightly increased by a longer aging time and slightly decreased by adding the mulberry leaf extract.
3. Based on the SEM images, all the nano-HA powders presented as rod-like particle agglomerates with a size below 100 nm. For the HA crystals developed by adding mulberry leaf extract, the particle size increased from 46.7 nm in length and 13.3 nm in diameter to 66.7 nm in length and 20.0 nm in diameter with increasing aging time from 10 min to 24 h.
4. ICP-AES evaluations showed the presence of Ca (31.2 wt%), P (14.7 wt%), Mg (0.329 wt%), and Sr (0.038 wt%) in the HA synthesized from mulberry leaf extract.
5. All HA powders synthesized in the presence and absence of the mulberry leaf extract show similar FT-IR spectra. The carbonate peaks observed for the specimens closely matched those of A- and B-type carbonates, which could contribute to their low crystallinity.
6. In the DTA curve for the HA synthesized from adding mulberry leaf extract, the phase transformation of HA into the β-TCP phase was detected at around 847 °C, and the decomposition of HA/β-TCP to the α-TCP phase was observed above 1122 °C.

Acknowledgements The authors acknowledge the partial financial support of Ministry of Science and Technology of Taiwan (105-2218-E-390-002; 106-2218-E-390-001; 107-2218-E-390-001; 107-2218-E-390-007; 108-2218-E-390-002).

References

1. N. Kaneko, Y. Suzuki, R. Umeda, R. Namiki, C. Izawa, T.I. Fukazawa, M. Honda, T. Takei, T. Watanabe, M. Aizawa, J. Asian Ceram. Soc. **8**, 130 (2020)
2. L.L. Hench, J. Am. Ceram. Soc. **74**, 1487 (1991)
3. A.E. Khouri, A. Zegzouti, M. Elaatmani, F. Capitelli, Inorg. Chem. Commun. **110**, 107568 (2019)
4. S. Dasgupta, S. Tarafder, A. Bandyopadhyay, S. Bose, Mater. Sci. Eng. C **33**, 2846 (2013)
5. A.P. Shpak, V.L. Karbovskii, A.G. Vakh, J. Electron. Spectrosc. **585**, 137 (2004)
6. S. Kannan, A. Rebelo, J.M.F. Ferreira, J. Inorg. Biochem. **100**, 1692 (2006)
7. W. Kong, K. Zhao, C. Gao, Mater. Lett. **255**, 126552 (2019)
8. G. Zuo, Y. Wan, L. Wang, C. Liu, F. He, H. Luo, Mater. Lett. **64**, 2126 (2010)
9. P. Zhang, Z. Hong, T. Yu, X. Chen, X. Jing, Biomaterials **30**, 58 (2009)
10. C.-H. Hou, S.-M. Hou, Y.-S. Hsueh, J. Lin, H.-C. Wu, F.-H. Lin, Biomaterials **30**, 3956 (2009)
11. S.C. Wu, H.C. Hsu, Y.N. Wu, W.F. Ho, Mater. Character. **62**, 1180 (2011)
12. W.F. Ho, H.C. Hsu, S.K. Hsu, C.W. Hung, S.C. Wu, Ceram. Inter. **39**, 6467 (2013)
13. S.C. Wu, H.C. Hsu, S.K. Hsu, Y.C. Chang, W.F. Ho, J. Asian Ceram. Soc. **4**, 85 (2016)
14. D. Liu, T. Troczynski, W.J. Tseng, Ceram. Inter. **22**, 1721 (2001)
15. S.C. Wu, H.K. Tsou, H.C. Hsu, S.K. Hsu, S.P. Liou, W.F. Ho, Ceram. Inter. **39**, 8183 (2013)
16. N. Roveri, G. Falini, M.C. Sidoti, A. Tampieri, E. Landi, M. Sandri, B. Pama, Mater. Sci. Eng. C **23**, 441 (2003)
17. X. Liu, L.A. Smith, J. Hu, P.X. Ma, Biomaterials **30**, 2252 (2009)
18. M. Gungormus, M. Branco, H. Fong, J.P. Schneider, C. Tamerler, M. Sarikaya, Biomaterials **31**, 7266 (2010)
19. K. Doi, T. Kojima, Y. Fujimoto, Biol. Pharm. Bull. **23**, 1066 (2000)
20. Y. Shibata, N. Kume, H. Arai, K. Hayashida, A. Inui-Hayashida, M. Minami, E. Mukai, M. Toyohara, A. Harauma, T. Murayama, T. Kita, S. Hara, K. Kamei, M. Yokode, Atherosclerosis **193**, 20 (2007)
21. E. Landi, A. Tampieri, G. Celotti, S. Sprio, J. Eur. Ceram. Soc. **20**, 2377 (2000)
22. M.H. Fathia, A. Hanifia, V. Mortazavi, J. Mater. Process. Technol. **202**, 536 (2008)
23. H.M. Kim, Y. Kim, S.J. Park, C. Rey, H.M. Lee, M.J. Gimcher, J.S. Ko, Biomaterials **21**, 1129 (2000)
24. M.S. Sadjadi, M. Meskinfam, B. Sadeghi, H. Jazdarreh, K. Zare, Mater. Chem. Phys. **124**, 217 (2010)
25. B. Ebrahimi-Kahrizsangi, A. Nasiri-Tabrizi, Chami. Solid State Sci. **12**, 1645 (2010)
26. X. Zhu, Y. Masuda, K. Koumoto, Biomaterials **25**, 3915 (2004)
27. K.D. Son, Y.-J. Kim, Mater. Sci. Eng. C **33**, 499 (2013)

28. Y. Deng, Y. Sun, X. Chen, P. Zhu, S. Wei, Mater. Sci. Eng. C **33**, 2905 (2013)
29. S. Mollazadeh, J. Javadpour, A. Khavandi, Ceram. Inter. **33**, 1579 (2007)
30. G. Balasundaram, M. Sato, T.J. Webster, Biomaterials **27**, 2798 (2006)
31. R. Murugan, S. Ramakrishna, Acta Biomater. **2**, 201 (2006)
32. S. Cazalbou, C. Combes, D. Eichert, C. Rey, J. Mater. Chem. **14**, 2148 (2004)
33. W.L. Suchanek, K. Byrappa, P. Shuk, R.E. Riman, V.F. Janas, K.S. TenHuisen, Biomaterials **25**, 4647 (2004)
34. A. Hoppe, N.S. Güldal, A.R. Boccaccini, Biomaterials **32**, 2757 (2011)
35. J. Braux, F. Velard, C. Guillaume, S. Bouthors, E. Jallot, J.M. Nedelec, D. Laurent-Maquin, P. Laquerrière, Acta Biomater. **7**, 2593 (2011)
36. C. Capuccini, P. Torricelli, F. Sima, E. Boanini, C. Ristoscu, B. Bracci, G. Socol, M. Fini, I.N. Mihailescu, A. Bigi, Acta Biomater. **4**, 1885 (2008)
37. E. Gentleman, Y.C. Fredholm, G. Jell, N. Lotfibakhshaiesh, M.D. O'Donnell, R.G. Hill, M.M. Stevens, Biomaterials **31**, 3949 (2010)
38. K. Prabakaran, S. Rajeswari, Spectrochim. Acta A **74**, 1127 (2009)
39. S. Koutsopoulos, J. Biomed. Mater. Res. **62**, 600 (2002)
40. I.K. Januariyasa, I.D. Ana, Y. Yusuf, Mater. Sci. Eng. C **107**, 110347 (2020)
41. A. Matsuura, T. Kubo, K. Doi, K. Hayashi, K. Morita, R. Yokota, H. Hayashi, I. Hirata, M. Okazaki, Y. Akagawa, Dent. Mater. J. **28**, 234 (2009)
42. S.J. Kalita, S. Verma, Mater. Sci. Eng. C **30**, 295 (2010)
43. M. Tămăşan, L.S. Ozyegin, F.N. Oktar, V. Simon, Mater. Sci. Eng. C **33**, 2569 (2013)
44. J. Peña, M. Vallet-Regí, J. Eur. Ceram. Soc. **23**, 1687 (2003)
45. R. Enderle, F. Götz-Neunhoeffer, M. Göbbels, F.A. Müller, P. Greil, Biomaterials **26**, 3379 (2005)